JHK Magnitudes for L and T Dwarfs and Infrared Photometric Systems

D.C. Stephens

Space Telescope Science Institute, Baltimore, MD 21218

stephens@stsci.edu

and

S.K. Leggett

Joint Astronomy Centre, University Park, Hilo, HI 96720

s.leggett@jach.hawaii.edu

ABSTRACT

In the last few years a significant population of ultracool L and T dwarfs has been discovered. With effective temperatures ranging from $\sim$ 2200 to 700 K, these objects emit most of their radiation in the near infrared and their spectral energy distributions are dominated by strong molecular absorption bands. These highly structured energy distributions lead to JHK magnitudes that are extremely sensitive to the exact filter bandpass used. In the case of the T dwarfs, the differences between commonly used photometric systems can be as large as 0.4 mag at J and 0.5 mag at $J-K$.

Near–infrared magnitudes have been published for L and T dwarfs using a variety of photometric systems. Currently, the data obtained with these systems cannot be accurately compared or combined as transformations based on the colors of hotter stars are not valid for L and T dwarfs. To address this problem, we have synthesized J, H, and K magnitudes for some of the common photometric systems and present transformation equations with respect to the most atmospheric–independent system, the Mauna Kea Observatory (MKO) filter set. If the spectral type of the dwarf is known, our transformations allow data to be converted between systems to 0.01 mag, which is better than the typical measurement uncertainty. Transforming on the basis of color alone is more difficult because of the degeneracy and intrinsic scatter in the near–infrared colors of L and T dwarfs; in this case J magnitudes can only be transformed to $\lesssim$0.05 mag and H and K to $\lesssim$0.02 mag.

Subject headings: stars: low-mass, brown dwarfs, fundamental parameters (magnitude, colors) – methods: data analysis

1. Introduction

L and T dwarfs have unusual spectral energy distributions (SEDs), with most of their flux emitted through windows in the near–infrared. Normalized spectra of an L5 and T4.5 dwarf (Geballe et al. 2002) are shown in Figure 1 to illustrate how absorption bands of H_2O, CO, and CH_4 regulate the near–infrared emission and create the flux windows. The H_2O bands are the same features responsible for the telluric absorption that defines the conventional J (1.1—1.4 μm), H (1.5—1.8 μm), and K (2.0—2.4 μm) bandpasses. Thus, the presence of H_2O in the atmospheres of the L and T dwarfs forces much of their flux to be emitted within these bands, resulting in the extreme far–optical and near–infrared colors that are used to identify L and T dwarf candidates from photometric surveys like the 2 Micron All Sky Survey (2MASS, Beichman et al. 1998), and the Sloan Digital Sky Survey (SDSS, York et al. 2000).

There are now hundreds of L and T dwarfs with near–infrared magnitudes published in various photometric systems. To maximize the science potential of these observations and their impact on brown dwarf theory, transformation equations are desirable to convert these and any future magnitudes to a common photometric system. Because the J, H and K bandpasses include H_2O, CO, and CH_4 absorption features, any variation in the width of the filters will lead to system–dependent magnitudes. Therefore, transformation equations need to be derived as a function of near–infrared spectral type or, less desirably, color (see later discussion in §4) to correctly account for the presence of the molecular bands.

Figure 2 shows $J-K$ color as a function of spectral type for typical main sequence stars (A0–M5) in the Bruzual–Persson–Gunn–Stryker Atlas[1], and late M, L and T dwarfs reported in Leggett et al. (2002). Important features to note, all of which are explained more fully in other works (e.g. Leggett et al. 2002) are: the intrinsic spread in $J-K$ for the L dwarfs that may be produced by variations in the extent and location of the condensed grain layer in the photosphere; the increasingly bluer $J-K$ color for the late L dwarfs and T dwarfs that is mostly due to the appearance of the CH_4 band at 2.2μm; and the scatter in $J-K$ for the latest T dwarfs likely due to gravity–dependent H_2 opacity. Although T dwarfs can have the same value of $J-K$ as A through M stars, convolving a T dwarf spectrum with its strong molecular absorption bands (Figure 1) with any JHK bandpass will produce a very different result from the convolution of e.g. the Rayleigh Jeans curve of an A0 star with the bandpass. Consequently, transformations based on the colors of hotter stars are not valid for L and T dwarfs and photometric transformations must be derived directly from observations of these ultracool dwarfs.

In this paper we present synthesized J, H and K magnitudes using near–infrared spectroscopic observations of L and T dwarfs from each spectral subtype, for the photometric systems in which L and T dwarf photometry has most frequently been published and for established systems in which future observations may occur. The photometric systems presented are: 2MASS (Carpenter

[1]http://www.stsci.edu/instruments/observatory/cdbs/astronomical_catalogs.html

2001), Caltech (CIT, Elias et al. 1982), the DEep Near-Infrared Survey (DENIS, Fouqué et al. 2000), Las Campanas Observatory (LCO, Persson et al. 1998), Mauna Kea Observatory (MKO, Simons & Tokunaga 2002; Tokunaga et al. 2002), the United States Naval Observatory Flagstaff Station (NOFS, Dahn et al. 2002; Guetter et al. 2003) and the United Kingdom Infrared Telescope (UKIRT, Hawarden et al. 2001). We also generate equations to transform J, H and K magnitudes between the other systems and the MKO system. The MKO photometric system was chosen as the reference point because MKO filters are narrower than classical J, H and K filters, thus avoiding the telluric absorption bands that can vary with time and observing location (see discussion in Simons & Tokunaga 2002, Tokunaga et al. 2002). As a result MKO magnitudes have little dependence on local observing conditions, and their use produces transformation equations with less uncertainty than would be obtained using another photometric system. In addition, the MKO filters have been widely adopted and the system is endorsed by the IAU Working Group on Infrared Photometry as the preferred photometric system for ground-based near–infrared observations.

In §2 we present the observed differences in the 2MASS and MKO magnitudes that have been measured for several L and T dwarfs, showing that system transformations cannot be reliably derived empirically due to significant uncertainty in the observational data. §3 discusses the inputs for synthesizing magnitudes: filter transmission profiles, telluric absorption bands, instrument optics and observed spectra. Our results are presented in §4 and our conclusions given in §5.

2. Observed Magnitudes in Different Systems

Figures 3 and 4 compare the J, H and K magnitudes, and $J-H, H-K$ and $J-K$ colors for a sample of L and T dwarfs that have been observed in both the 2MASS and MKO photometric systems. These are the only systems with a large enough number of L and T dwarfs in common to make a meaningful observational comparison. 2MASS magnitudes for these objects were taken from the 2MASS L dwarf archive webpage[2] and A. Burgasser's T dwarf webpage[3]. The MKO magnitudes are reported in Leggett et al. (2002). Figure 3 plots δmag as a function of spectral type and Figure 4 plots δmag as a function of $J-K$ (on the MKO system), which provides the largest baseline.

Spectral type is taken from Geballe et al. (2002), who define a classification scheme for both L and T dwarfs based on the strength of the near–infrared absorption bands. This classification gives results very similar to the scheme presented for the T dwarfs by Burgasser et al. (2002). However, the scheme for L dwarfs presented by Kirkpatrick et al. (2000), which is based on red spectra, can assign L dwarf spectral types that differ by up to 2.5 subclasses from the Geballe classification. For the samples shown in Figures 3 and 4 the average difference in L dwarf classification is only 1.0

[2]http : //spider.ipac.caltech.edu/staff/davy/ARCHIVE/index_l_spec.html

[3]http : //www.astro.ucla.edu/ ∼ adam/homepage/research/tdwarf/

subclass. Therefore, given the size of the observational uncertainty (see the Figures) the choice of classification scheme is not significant.

Despite the large observational uncertainty in Figures 3 and 4, it can be seen that there are significant differences in the magnitudes, especially at J, and that general trends in δmag with type do exist. The difference between systems can be understood with reference to the spectra shown in Figure 1. The 2MASS J filter is wider than the MKO J and 2MASS K is narrower than MKO K (§3.1); the wider filters include more of the absorption bands of H_2O and CH_4 without increasing the signal, and hence, with reference to the calibrator, L and T dwarfs appear to be fainter in the systems with wider filters. As these features become stronger with later spectral type, the effect is more pronounced and trends appear with 2MASS J becoming increasingly fainter than MKO J, and MKO K fainter than 2MASS K. Although these trends can be seen, the considerable uncertainty in the data prevents the determination of reliable system transformations from direct observations. In the following sections we derive and discuss theoretical transformations between these and other systems.

3. Calculation of Synthetic Magnitudes

3.1. Filters

Figure 5 shows the filter profiles for the 2MASS, CIT, DENIS, LCO, MKO, NOFS and UKIRT JHK filters at instrument temperatures. The 2MASS filter profiles were obtained from the 2MASS webpages[4], the MKO filter profiles were obtained from the UKIRT webpages[5] and the UKIRT profiles from Hawarden et al. (2001). The LCO profiles were generated with tables obtained from Persson et al. (1998), the DENIS profiles were obtained from P. Fouqué (priv. comm. 2002) and the NOFS profiles were obtained from F. Vrba (priv. comm. 2003). The CIT–H and K profiles measured at operating temperature were obtained from the CTIO infrared instrumentation webpage[6], where they are identified as 25mm OCLI H and K filters. We selected these filters for CIT–H and K because they match the documented CIT bandpasses (Elias et al. 1982). The CIT–J profile measured at ambient temperature was also obtained from the CTIO webpage, where it is identified as CIT–J. A shift to bluer wavelengths was required to correct this profile to values appropriate for operating temperatures.

We attempted to determine the appropriate shift for the CIT–J band from the literature, however there is a discrepancy between the cold transmission profile measured for CIT–J by H. Jones (private comm. between E. Persson and H. Jones 1994; Jones et al. 1994) and the bandpass

[4]http : //www.ipac.caltech.edu/2mass/releases/second/doc/sec3_1b1.html

[5]http : //www.jach.hawaii.edu/JACpublic/UKIRT/instruments/uist/imaging/filters.html

[6]http : //www.ctio.noao.edu/instruments/ir_instruments/irfilters/filters.html

given by Elias et al. (1982). Therefore, two independent shifts were made to the CIT–J bandpass, producing two different transmission profiles. The first shift moved the bandpass ∼0.015 μm and was chosen to produce a bandpass identical to the one determined for the CIT system by H. Jones. We refer to this filter bandpass as CIT–J throughout the rest of the paper (solid line in Figure 5). The second J bandpass was created by shifting the ambient J profile ∼0.04 μm to match the CIT–J bandpass specified by Elias et al. (1982). In determining this shift, we assume that the Elias et al. (1982) bandpass limits do not include atmosphere (see §3.2) and we refer to this bandpass in the paper as Elias–J (dash–dot line in Figure 5).

Since the original 1980–era CIT filter profiles no longer exist (J. Elias and E. Persson, private comm. 2003), it is not clear which transmission profile represents the original CIT–J filter. The Elias–J bandpass involves a ∼3% shift in wavelength of the webpage ambient profile, which is about twice the value seen for the UKIRT filters on a cooldown from ambient to 77K. In this regard, the bandpass measured by Jones seems more reasonable. However, we present both profiles in this work as the bluer bandpass is specified in the defining work by Elias et al. (1982). Note that the red cut-off of each filter is effectively defined by the atmosphere, but the differences in the blue cut–on produces significant systematic differences in the J magnitudes, as we show in §4. The H and K magnitudes are well determined as these profiles agree with the Elias et al. (1982) bandpasses and are identical to the CIT profiles measured by H. Jones (private comm. 1994; Jones et al. 1994).

3.2. Atmospheres

Figure 5 shows as a dotted line the effective bandpass of each filter after convolving with the atmospheric transmission appropriate for each site. For 2MASS and NOFS the mean transmission of Mount Hopkins (which appears to be equivalent to a little more than 5mm water) was used (Carpenter 2001). For CIT, Elias–J (dashed line), DENIS, and LCO an atmosphere profile typical of Las Campanas was obtained from the Las Campanas WIRC Users Manual webpage[7]. For UKIRT and MKO the 1.2 mm Mauna Kea atmosphere was used. The Mauna Kea atmosphere for various values of water vapor have been calculated by the ATRAN model (Lord 1992) and are available from the Gemini webpages[8]. An atmosphere profile typical of conditions at Cerro Tololo was also obtained that could have been used with the CIT filters instead of the LCO atmosphere. However, the difference in synthetic CIT magnitudes produced from the two atmospheres was negligible for H and K, and never more than 0.005 mag at J for the L dwarfs and 0.009 mag at J for the T dwarfs.

Figure 5 shows that all but the LCO and MKO J filter bandpasses extend into poor regions of the atmosphere, usually by being too red (although the 2MASS, DENIS and NOFS filters are also

[7]http : //www.ociw.edu/instrumentation/wirc/wirc.html

[8]http : //www.gemini.edu/sciops/ObsProcess/obsConstraints/ocTransSpectra.html

too blue). Carpenter (2001) states that the 2MASS J–band calibration zero points often showed variations within a night as large as 0.1 mag, most likely due to variations in the atmosphere (however colors were stable to <0.02 mag). To explore the effect of variable water vapor on the J magnitude, we synthesized photometry for each system using different amounts of water vapor. We found that if the water vapor is varied between 1 mm and 3 mm, the UKIRT J magnitudes differ by 0.01 mag for mid–L dwarfs, 0.02 mag for late–Ls, 0.03 mag for early–Ts, and 0.05 mag for late–T dwarfs. If the water vapor is varied between 3 mm and the mean transmission at Mount Hopkins (∼5mm), the 2MASS J magnitudes differ by 0.03 mag for the early– to mid–L dwarfs, 0.04 mag for the late–Ls, and from 0.05 mag up to 0.1 mag for the T dwarfs. The dependence of the J magnitude on the atmospheric transmission highlights the need for a bandpass that is free of the atmosphere (see also further discussion in Simons & Tokunaga 2002, Tokunaga et al. 2002).

3.3. Detector and Optical Responses

The filter profiles shown in Figure 5 do not include the effect of other optical elements in the instrument lightpath. Telescope mirrors, instrument optics and the detector quantum efficiency (QE) will produce wavelength–dependent transmission or reflection curves which should, strictly, be convolved with the filter and atmosphere transmission. We have investigated the effect of various commonly used elements and show below that they are negligible; therefore, we calculate synthetic magnitudes using the filter and atmosphere transmissions only.

The commonly used reflective surfaces in a near–infrared telescope will be gold, silver or aluminum. The reflection curves of these surfaces are flat within measurement uncertainty from 1.0 to 2.6 μm, at 94 to 98%. The commonly used transmissive elements are zinc selenide, and calcium, lithium or barium fluoride. Uncoated, such windows or lenses have flat transmissions at 94 to 95%. Anti–reflection (AR) coatings can lead to a wavelength–dependent response, however the coatings for infrared instrument are usually optimized for the near–infrared and the lens coatings in the UKIRT cameras for example vary in throughput by only 1%, typically, across any of the J, H or K bandpasses.

A more serious issue is variations in detector QE, in particular large variations in the AR coatings on detectors. We have found that current 1024×1024 InSb ALADDIN arrays have a more structured reflectivity curve than older generation InSb detectors. UKIRT's ALADDIN detector in the UIST camera has a curve that varies in reflectivity from 10 to 20% across the J filter for example, while the older 256×256 InSb detector in IRCAM is reasonably flat with a ≤2% change across any filter bandpass. Carpenter (2001) indicates that the 2MASS NICMOS detector QE is quite flat at 60 to 65% across J, H and K. Given the highly structured SEDs of the L and T dwarfs we investigated the impact of the detector coatings by calculating synthetic magnitudes for the MKO filter set with and without the ALADDIN–type coating. We find the effect to be 0.01 mag at J for mid–L through T types, 0.002 mag at H, and 0.003 mag at K except for late T dwarfs where the difference is 0.01 mag at K. Measurement uncertainties are always significantly larger

than these values, hence it appears that AR coatings, while important for instrument throughput, have a negligible effect on photometric systems, even for L and T dwarfs.

3.4. Spectra

Magnitudes were synthesized by convolving observed flux–calibrated spectra across the filter+atmosphere bandpasses, and calibrated by convolving these same bandpasses with the observed energy distribution of Vega (Hayes 1985; Mountain et al. 1985) which was assumed to have zero magnitude at each bandpass. The L and T dwarf spectra were taken from Geballe et al. (2002), supplemented by additional data on 2MASS0415−09 and SDSS1110+01 (Knapp et al. 2004). The noise in the L and T dwarf spectra was typically 2% of the flux at J (rising to 4% for the ∼30% of the sample with $J \approx 17$), 1% at H (rising to 2% for the faintest dwarfs), and 3% at K (rising to 4%). The uncertainty in the absolute flux calibration of Vega is estimated to be 3% in the near–infrared. However the uncertainty in the Vega calibration and in the input spectra can be neglected here. The uncertainty in the the flux calibration of the L and T dwarf spectra will be predominantly due to the uncertainty in the photometry used to originally calibrate the spectra, which is 3–5% (Leggett et al. 2002)[9].

We found when deriving the synthetic magnitudes that more consistent results were obtained if the filter bandpasses all had the same, high resolution. Therefore we resampled each filter profile to $\delta\lambda$ =0.001 μm before convolving with the atmosphere. The bandpasses used in this work, with and without the atmosphere (see §3.2), are available on request from the authors; they can be used to derive magnitudes in various photometric systems from a flux–calibrated near–infrared spectrum, provided the spectrum covers the full bandpass of the filter.

We also found that unless we had spectra that covered the complete bandpass, additional scatter was introduced into our magnitude comparisons. This was only an issue for the J filters as most of the spectra did not go into the poor transmission region around 1.35 μm. If incomplete spectra were used, errors were introduced in the synthetic magnitudes as large as 0.1—0.4 mag for the UKIRT filter, which has significant transmission at 1.35 μm. For the other wide J–band filters the effect was smaller, typically 0.02 to 0.04 mag. We corrected the spectra by interpolating the

[9]The observed magnitude m_o measured with a filter+atmosphere profile t_o is used to scale the input spectrum f_* by a constant c such that

$$10^{-0.4m_o} = c * \frac{\int f_* t_o \delta\lambda}{\int f_{Vega} t_o \delta\lambda}$$

then the derived magnitude m' is determined by

$$10^{-0.4m'} = 10^{-0.4m_o} * \frac{\int f_* t' \delta\lambda}{\int f_* t_o \delta\lambda} * \frac{\int f_{Vega} t_o \delta\lambda}{\int f_{Vega} t' \delta\lambda}$$

While the absolute flux of Vega is uncertain at the 3% level, the slope across the filter is well determined. The noise in the dwarf spectrum is only significant where it is differently weighted by the two filter profiles. Hence the uncertainty in the synthetic magnitude is driven by the uncertainty in m_o.

data across the gap using as templates bright dwarfs that had been observed in this spectral region on Mauna Kea. Tests using a variety of templates show that the uncertainty introduced in the J magnitude by this interpolation is $\lesssim$5 millimags for the wider filters, such as the UKIRT filter.

4. Results

Tables 1, 2 and 3 list the synthesized J, H and K magnitudes, respectively, in the various systems for the sample of 24 L dwarfs and 17 T dwarfs. The magnitudes are given to the millimag level despite the 0.03–0.05 mag uncertainty in these derived magnitudes because we wish to avoid introducing errors in the transformations by rounding off the synthetic magnitudes to too low a level of significance. The transformations are given by the difference in magnitudes from each system and as systematic errors in the flux calibration cancel out, the uncertainty in this difference is smaller than that in the original photometry. The uncertainty in the transformation is determined only by the weighting of the noise in the spectra by each bandpass, and also by any uncertainty in the definition of the bandpass (see §3.1, 3.2, 3.4 and further discussion below).

Figure 6 shows the calculated differences in JHK for the various photometric systems as a function of spectral type, and Figure 7 the difference in the colors as a function of type. Figures 8 and 9 also show δmag and δcolor, this time as a function of $J - K_{MKO}$. The trends in δ(2MASS−MKO) agree well with the observed trends shown in Figures 3 and 4. Other observational comparisons are very limited. Only three L dwarfs have independently measured J and K in both the DENIS and MKO systems and for these the agreement with Figure 6 is reasonable, but the observational uncertainties are large. No data currently exists in the LCO system for L and T dwarfs. Data have been published for some dwarfs in both the UKIRT and MKO systems, but these are not independent measurements, instead one dataset has been synthesized from the other as we have done here. Photometry for several L and T dwarfs obtained with the NOFS filters has been published by Dahn et al. (2002) and calibrated using Elias et al. (1982) standards (Guetter et al. 2003). Comparison of the NOFS–system magnitudes with MKO data for 15 L dwarfs and two T dwarfs in common produces δmags which agree well with our derived sequences at J and H, but which differ at K for the two T dwarfs by $\sim$0.2 mag (compared to the measurement uncertainty of $\sim$0.1 mag). These results will be investigated further when more data from this group are available.

In Figures 6 and 7 spectral type is given on the infrared typing scheme of Geballe et al. (2002). As discussed in §2, the optically–based L dwarf classification scheme of Kirkpatrick et al. (2000) can lead to differences in spectral classification of up to 2.5 subclasses, although the average difference for this sample is only 1.0 subclass. The uncertainty in the Geballe classification is typically 0.5 subclasses, and, given the slow change in δmag with type for L dwarfs, the sequences shown in Figures 6 and 7 should be effectively independent of the classification scheme. We tested this by fitting δmag values using both the Geballe and Kirkpatrick classifications and the difference for a given L type was always substantially less than the standard deviation of the fit.

As an additional check, we determined the difference in δmag that would occur if spectral type was allowed to vary by two L sub-classes, simulating the difference in classification that can occur between the visible and near-infrared classification systems. For the case of the 2MASS J filter, which is a relatively steep function of type, the difference in δmag between L6 and L8 types is 0.017 mag. The sensitivity to type for earlier L spectral types is <0.01 mag, and the H and K filters are insensitive to L dwarf type as can be seen in Figure 6. Hence uncertainties in L spectral type lead to uncertainties in δmag of <0.01 mag except for late L dwarfs at J where large uncertainties could lead to an uncertainty of ∼0.02 mag. Note that to determine near–infrared photometric system dependencies, an infrared scheme is more appropriate than an optical scheme and should give a tighter relationship between δmag and type.

The δmag:type sequences can be fit well mathematically. Table 4 gives the results of cubic fits to δJ, δH and δK as a function of type, all with respect to the MKO system, and the standard error of the fit in magnitudes (colors can be calculated by differencing the relations). The accuracy of the derived transformations are quite good — the standard error is better than 0.01 mag. The fits to δmag with type can be seen as solid lines in Figure 6. The scatter around the fits is small, 0.005–0.020 magnitudes, which is consistent with the noise in the spectra.

The δmag:$J-K$ relationship is more difficult to fit due to the degeneracy in colors between early L and T dwarfs, the degeneracy within the L dwarfs, and the intrinsic spread in JHK colors of L and T dwarfs with the same spectral type (§1, Figure 2). Objects with different spectral morphologies can have the same color, but will have different values for δmag. Consequently, transformations based on color alone will combine dwarfs with different spectral characteristics and produce a δmag value which will be less accurate than the value based on spectral type. This is a problem in particular for δJ, as a function of $J-K$, as can be seen in Figure 8. Tables 5 and 6 give the results of fits to δJ, δH and δK as a function of $J-K$ color in each of the photometric systems: Table 5 gives the coefficients for the quadratic fit found for δJ, and Table 6 gives the coefficients for δH and δK which were fit well with linear equations. These fits are shown as solid lines in Figure 8. The scatter around the fits at J is 0.005—0.070 mag, at H it is 0.003—0.030 mag and at K 0.015—0.030 mag. Thus H and K magnitudes can be transformed almost equally well using either spectral type or color, but J magnitudes transformed from color will be much more uncertain than those based on type. Separating the L and T dwarfs can produce better transformations for the J filter; these fits, and fits using other color combinations, can be determined using the synthetic magnitudes given in Tables 1—3.

To summarize, if the spectral type of the dwarf is known and the filter can be regarded as well determined, then J, H and K transformations can be determined to $\sim$ 0.01 mag using the equations provided in Table 4. Therefore for most observations the original measurement uncertainty (typically $\gtrsim$ 0.03 mag, see e.g. Figure 3) will limit the accuracy of the transformed magnitude . However other uncertainties do exist that can significantly effect the J magnitudes, or colors involving J. The CIT J bandpass is not well known, and the profiles of the wider J filters are determined by a possibly variable atmosphere; we showed in §3.2 that a plausible range

in water vapor levels can lead to variations in the J magnitudes of 0.05—0.10 mag for T dwarfs, for such filters. For late L dwarfs, an uncertainty in spectral type of 2 subclasses can lead to an uncertainty in $\delta J \sim 0.02$ mag. If the spectral type is not known at all, then transforming based on $J - K$ color leads to an uncertainty in $\delta J \sim 0.05$ mag. For mid–L through T types, variations between detectors can result in an additional, but small, uncertainty in $\delta J \sim 0.01$ mag (§3.3). The H and K bandpasses are better behaved. Detector response uncertainty is only expected to impact K and then only for late T dwarfs at the 0.01 mag level. Also, for H and K transformations can be derived to ~ 0.02 mag on the basis of color alone.

5. Conclusions

To obtain accurate and stable photometry, filter bandpasses should not go into poor regions of the terrestrial atmosphere — most (classical) J filters are poorly defined from this point of view. Variations in the water vapor content change the effective bandpass of such filters and, for objects with extremely structured spectral energy distributions such as T dwarfs, these changes produce photometric deviations of ∼0.05—0.10 magnitudes. To measure magnitudes and colors to better than this requires use of a filter set that is well matched to the atmosphere, such as the MKO filter set.

JHK magnitudes for L and T dwarfs are highly dependent on the photometric system used for the observation; for T dwarfs differences between systems can be several tenths of a magnitude. However, we have shown that JHK magnitudes for L and T dwarfs can be transformed between the 2MASS, CIT–$H\&K$, DENIS, LCO, NOFS and UKIRT systems and the MKO system to ∼0.01 mag if the spectral type of the dwarf is known. This is significantly better than the typical measurement uncertainty, i.e. the original uncertainty in the measurement will determine the accuracy of the transformed value. For the CIT system the uncertainty in the J bandpass effects the derived magnitudes by 0.05–0.10 mag for L and T dwarfs. Variations between the optical elements of common infrared instrumentation are expected to impact the measured magnitudes of the late L and T dwarfs at the 0.01 mag level. If spectral type is not known, then $J - K$ color can be used to transform H and K magnitudes measured in different systems with an accuracy of about 0.02 mag but the J value can only be derived to ~ 0.05 mag on the basis of color alone.

The results presented here will be valuable for researchers in the very active field of ultracool dwarf studies, where imaging data are plentiful, and where the data have unfortunately been obtained with a variety of photometric systems. Transformations based on the colors of hotter stars, even if the stars have the same color, cannot be applied to objects with strong molecular absorption bands such as those seen in L and T dwarfs. For these ultracool objects intercomparison of photometric data requires knowledge of the filter profiles at instrument temperature, and knowledge of the local atmospheric transmission. If JHK photometry is obtained with a well understood photometric system we have shown that such datasets can be accurately combined or compared.

We are grateful to Jill Knapp and colleagues for use of spectra prepublication, to Hugh Harris for useful discussions and to the referee Adam Burgasser for improvements to the paper. We thank all those responsible for setting up the 2MASS, DENIS and SDSS surveys, which enabled the discovery of the population of field L and T dwarfs.

REFERENCES

Beichman, C.A., Chester, T.J., Skrutskie, M., Low, F.J., & Gillett,F. 1998, PASP, 110, 480

Burgasser, A.J., et al. 2002, ApJ, 564, 421

Carpenter, J.M. 2001, AJ, 121, 2851

Dahn, C., et al. 2002, AJ, 124, 1170

Elias, J.H., Frogel, J.A., Matthews, K., & Neugebauer, G. 1982, AJ, 87, 1029

Fouqué, P., et al. 2000, A&AS, 141, 313

Geballe, T.R., et al. 2002, ApJ, 654, 466

Guetter, H.H., Vrba, F.J., Henden, A.A., & Luginbuhl, C.B. 2003, AJ, 125, 3344

Hawarden, T.G., Leggett, S.K., Letawsky, M.B., Ballantyne, D.R., & Casali, M.M. 2001, MNRAS, 325, 563

Hayes, D.S. 1985, IAU Symp, 111, 225

Jones, H.R.A., Longmore, A.J., Jameson, R.F., & Mountain, C.M. 1994, MNRAS, 267, 413

Kirkpatrick, J.D., et al. 2000, AJ, 120, 447

Knapp, G.R., et al. 2004, in prep

Leggett, S.K., et al. 2002, ApJ, 564, 452

Lord, S.D. 1992, NASA Technical Memor. 103957

Mountain, C.M., Selby, M.J., Leggett, S.K., Blackwell, D.E., & Petford, A.D. 1985, A&A, 151, 399

Persson, S.E., Murphy, D.C., Krzeminski, W., Roth, M., & Rieke, M.J. 1998, AJ, 116, 2475

Simons, D.A., & Tokunaga, A.T., 2002, PASP, 114, 169

Tokunaga, A.T., Simons, D.A., & Vacca, W.D. 2002, PASP, 114, 180

York, D.G., et al. 2000, AJ, 120, 1579

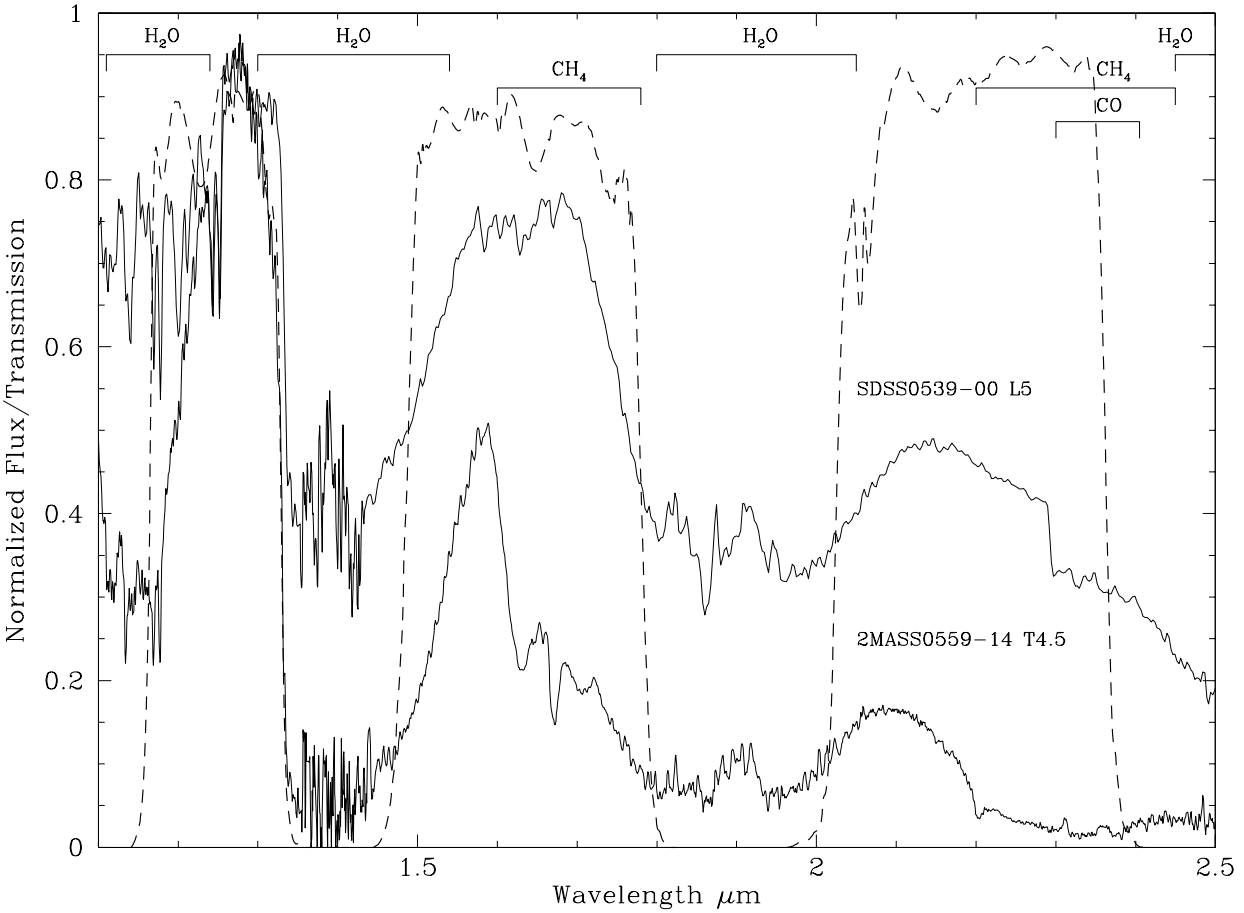

Fig. 1.— Normalized observed spectra for an L5 and a T4.5 dwarf from Geballe et al. (2002). The principal absorption bands in the dwarf spectra are identified and the bandpasses for the MKO J, H and K filters (left to right) are shown as dashed lines.

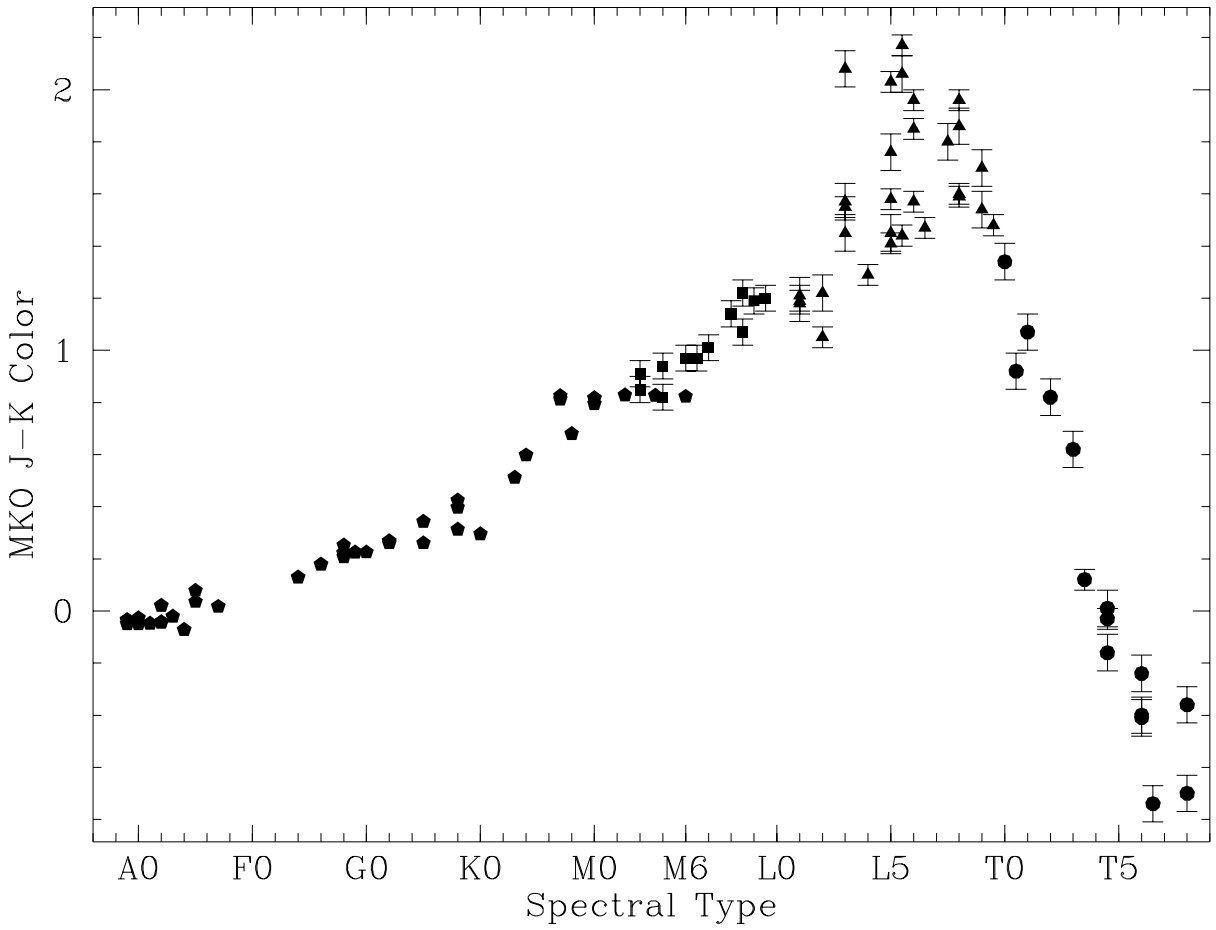

Fig. 2.— Observed MKO $J - K$ colors for several late M (squares), L (triangles) and T dwarfs (circles) as a function of spectral type (Leggett et al. 2002). Synthetic $J - K$ values generated for the standard main sequence stars in the Bruzual–Persson–Gunn–Stryker spectral atlas are also shown for comparison (pentagons).

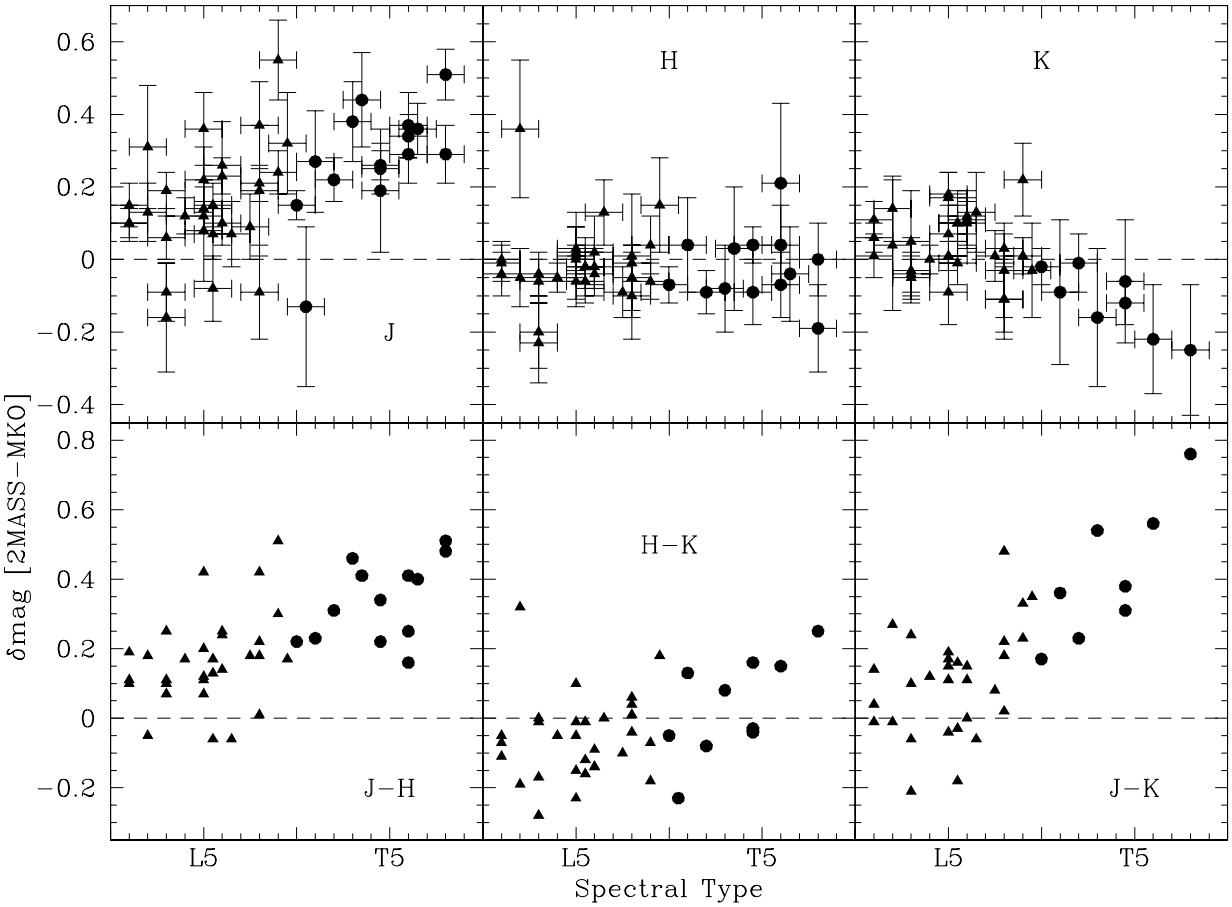

Fig. 3.— Observed δJ, δH, δK, $\delta(J-H)$, $\delta(H-K)$ and $\delta(J-K)$ mag, as a function of spectral type, for the 2MASS and MKO systems. L dwarfs are shown as triangles and T dwarfs as circles. Error bars are omitted in the lower plot for clarity.

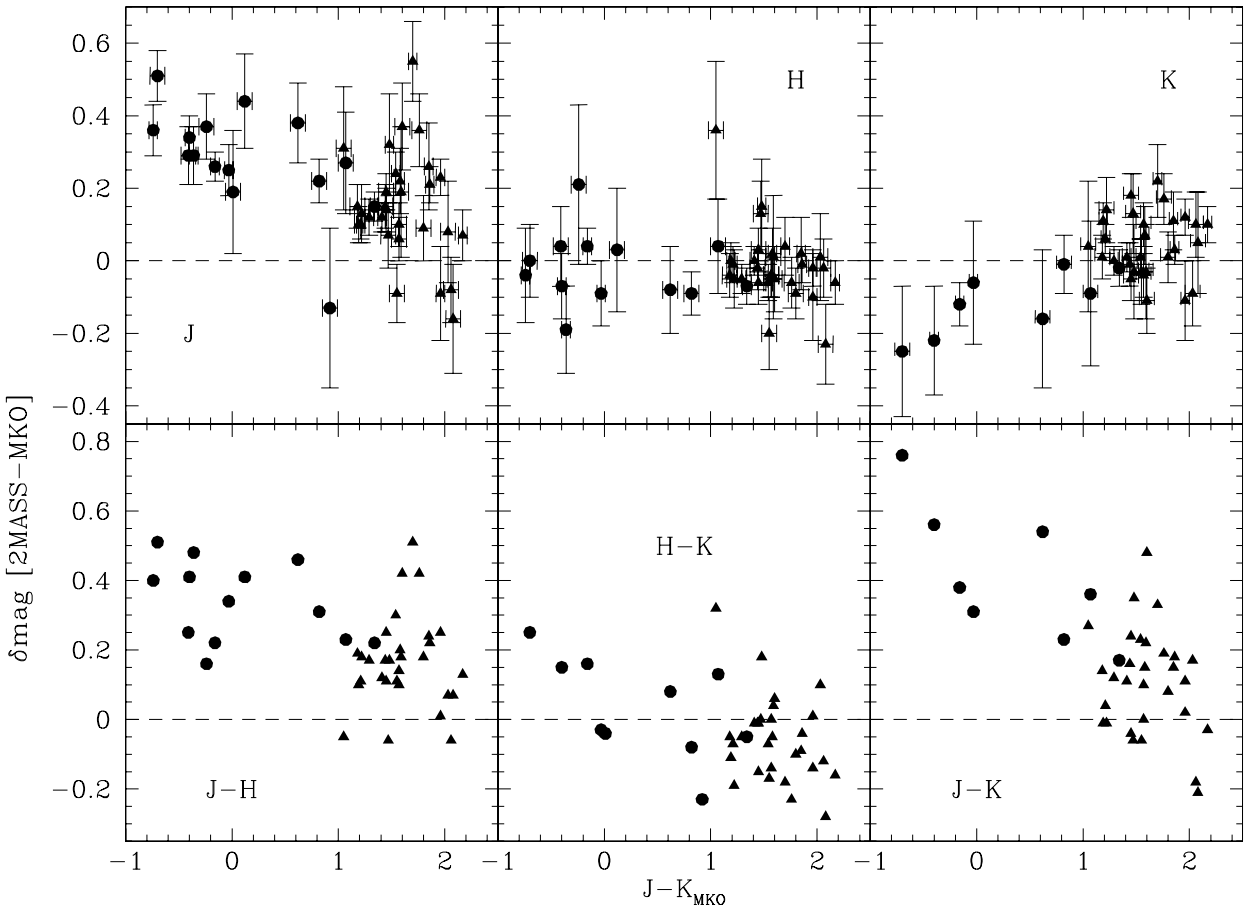

Fig. 4.— Observed δJ, δH, δK, $\delta(J-H)$, $\delta(H-K)$ and $\delta(J-K)$ mag, as a function of color, for the 2MASS and MKO systems. L dwarfs are shown as triangles and T dwarfs as circles. Error bars are omitted in the lower plot for clarity.

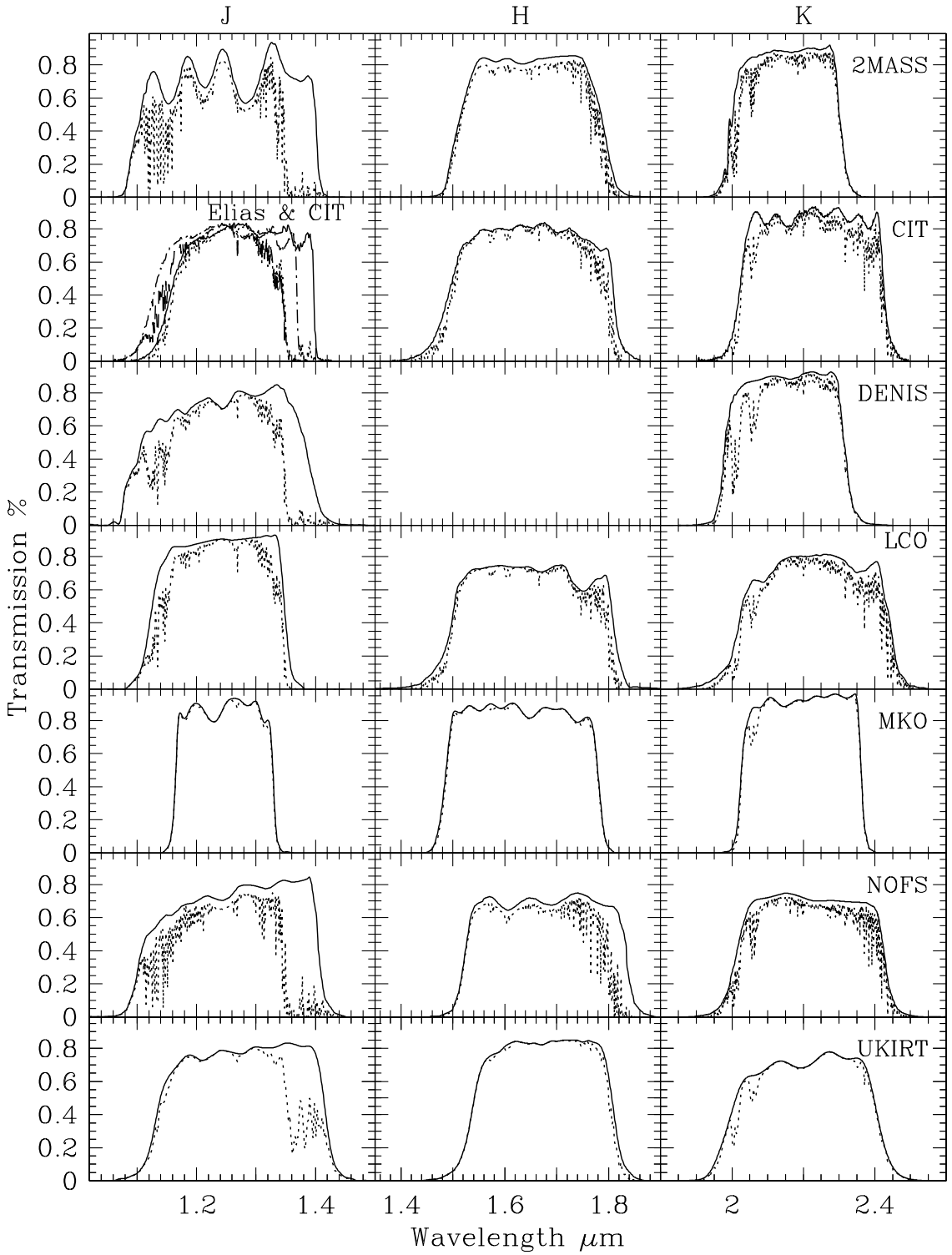

Fig. 5.— Filter bandpasses for the systems considered here (solid line) and with atmospheric absorption (dotted line). The Elias–J bandpass is drawn in the same box as the CIT–J bandpass, both without atmospheric absorption (dash-dot line) and with (dashed line).

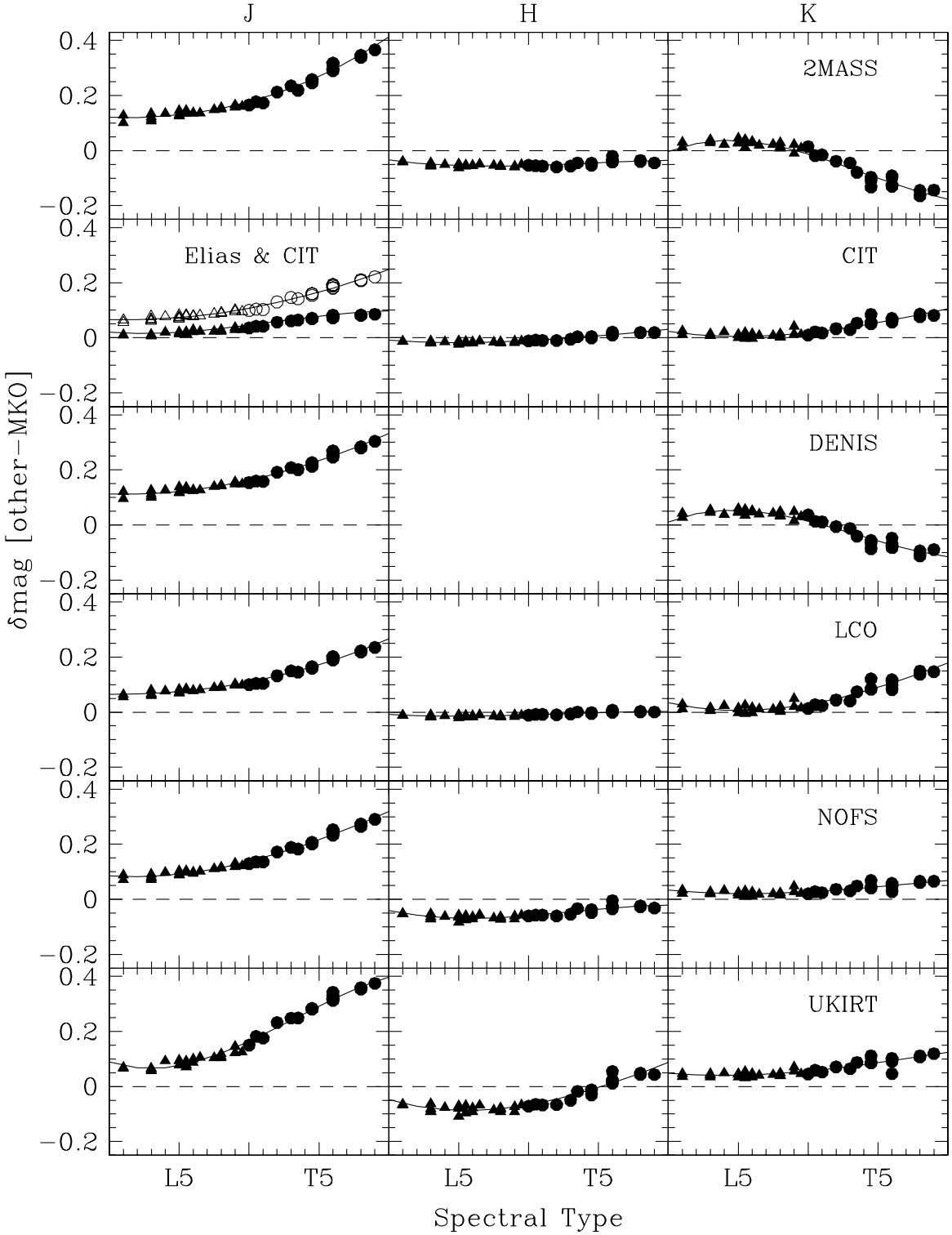

Fig. 6.— Synthesized δJ, δH and δK mag, as a function of spectral type for all the systems considered here. L dwarfs are shown as triangles and T dwarfs as circles. Synthesized δmags using the Elias–J filter are shown as open symbols. The solid lines show the cubic fits given in Table 4.

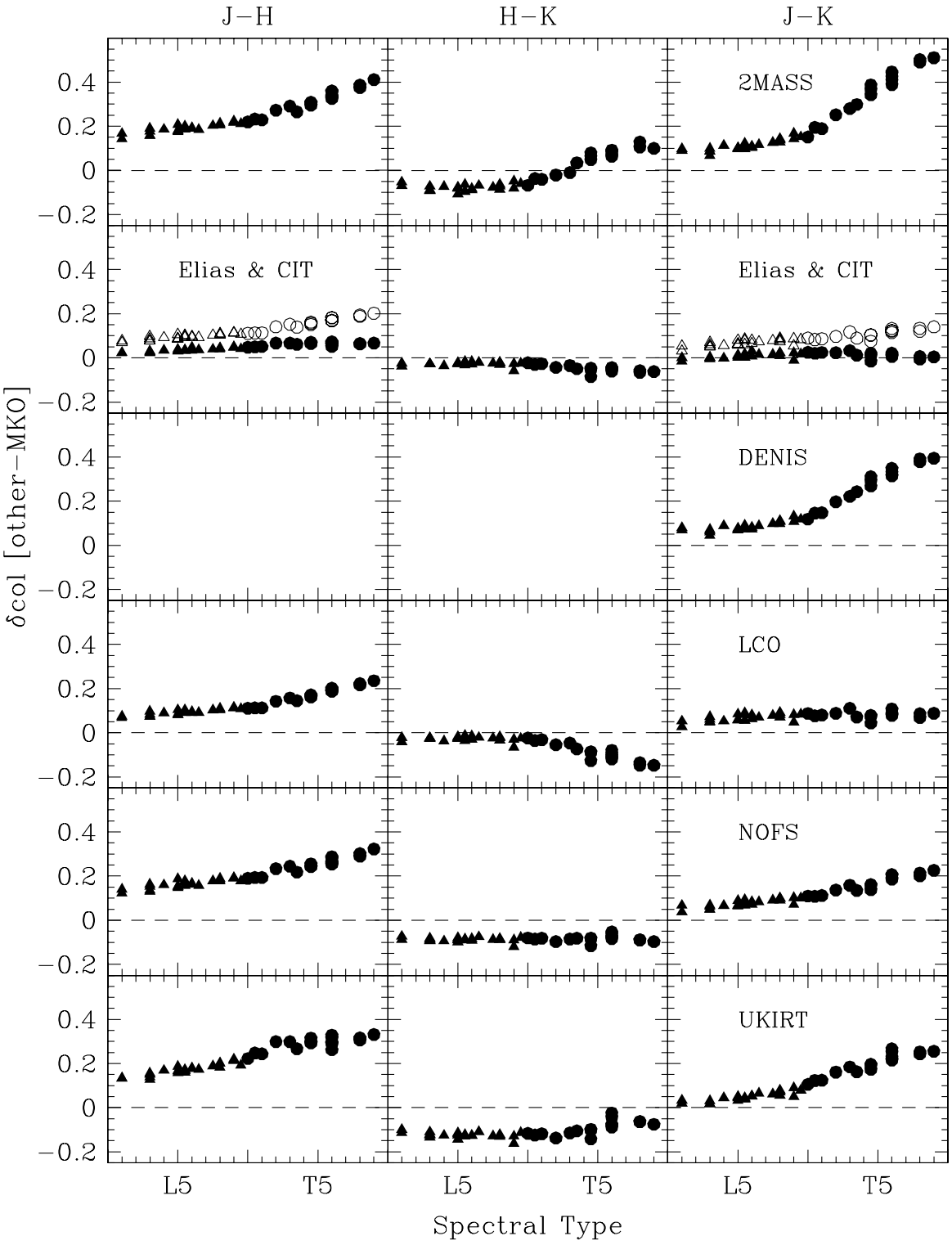

Fig. 7.— Synthesized $\delta(J-H)$, $\delta(H-K)$ and $\delta(J-K)$ mag, as a function of spectral type for all the systems considered here. Symbols are as in Figure 6.

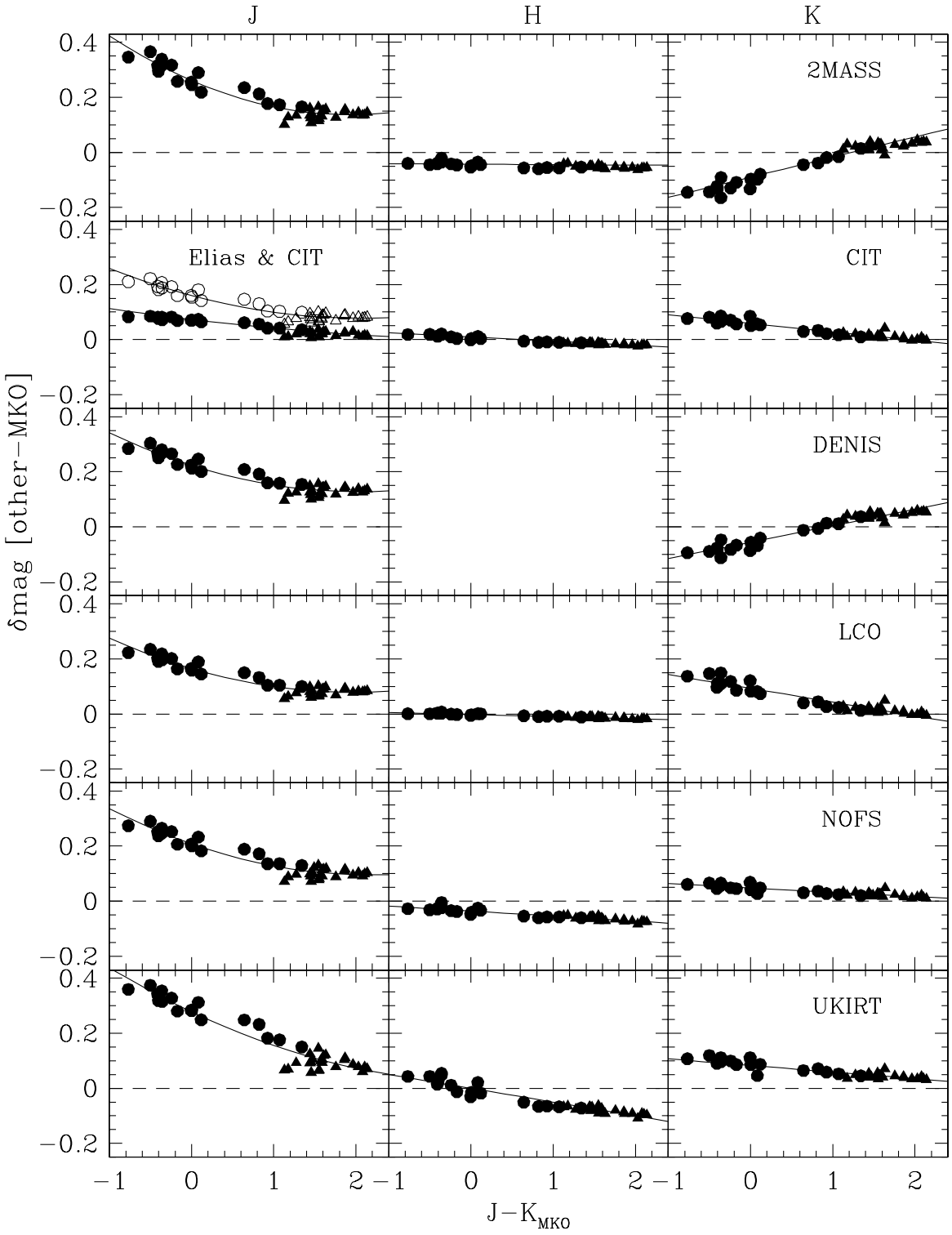

Fig. 8.— Synthesized δJ, δH and δK mag, as a function of color for all the systems considered here. Symbols are as in Figure 6. The solid lines show the fits given in Tables 5 and 6.

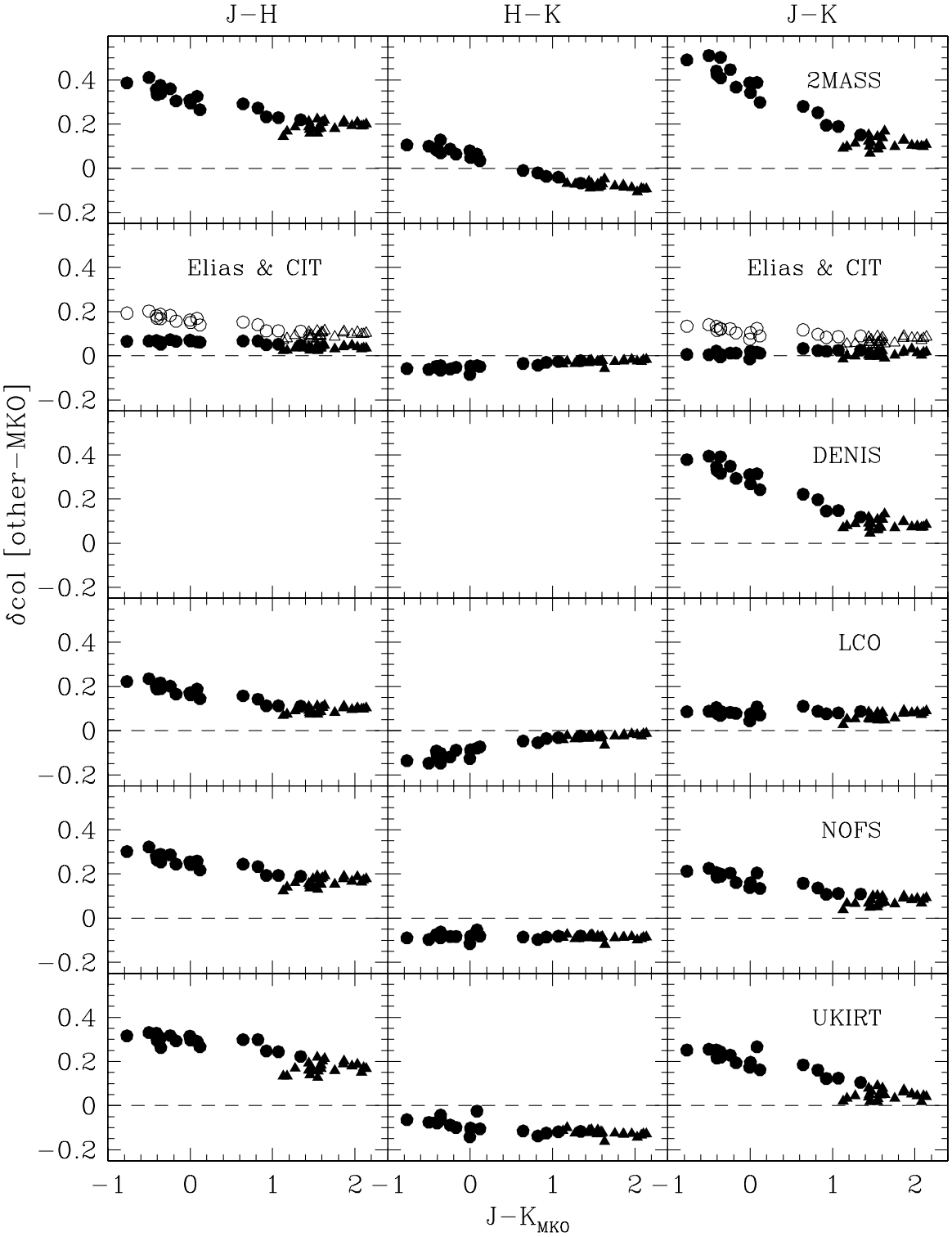

Fig. 9.— Synthesized $\delta(J-H)$, $\delta(H-K)$ and $\delta(J-K)$ mag, as a function of color for all the systems considered here. Symbols are as in Figure 6.

Table 1. Synthesized J-Band Photometry

Name	Type	2MASS	CIT	ELIAS	DENIS	LCO	MKO	NOFS	UKIRT
2MASS0345+25	L1	13.967	13.854	13.904	13.961	13.903	13.839	13.928	13.908
2MASS0746+20AB	L1	11.683	11.595	11.637	11.677	11.637	11.581	11.652	11.648
2MASS0028+15	L3	16.788	16.668	16.731	16.779	16.733	16.653	16.744	16.713
DENIS1058−15	L3	14.244	14.136	14.188	14.234	14.188	14.121	14.203	14.187
GD165B	L3	15.752	15.653	15.702	15.743	15.702	15.637	15.715	15.701
Kelu−1	L3	13.343	13.246	13.295	13.335	13.295	13.235	13.307	13.293
2MASS0036+18	L4	12.454	12.344	12.396	12.445	12.396	12.319	12.417	12.412
SDSS0539−00	L5	13.976	13.876	13.923	13.967	13.922	13.850	13.941	13.945
SDSS1257−01	L5	15.770	15.663	15.713	15.759	15.712	15.639	15.731	15.733
SDSS1446+00	L5	15.686	15.577	15.628	15.677	15.628	15.559	15.647	15.637
SDSS2249+00	L5	16.608	16.482	16.544	16.600	16.545	16.462	16.566	16.540
DENIS0205−11AB	L5.5	14.540	14.431	14.485	14.531	14.486	14.405	14.504	14.497
SDSS0107+00	L5.5	15.876	15.749	15.813	15.868	15.816	15.731	15.834	15.802
SDSS1326−00	L5.5	16.317	16.201	16.259	16.310	16.261	16.180	16.279	16.258
2MASS0825+21	L6	15.028	14.919	14.969	15.016	14.969	14.891	14.986	14.978
DENIS1228−15AB	L6	14.420	14.309	14.362	14.411	14.362	14.283	14.382	14.383
SDSS0236+00	L6.5	16.146	16.039	16.091	16.137	16.091	16.010	16.112	16.116
2MASS1632+19	L7.5	15.921	15.800	15.859	15.912	15.861	15.772	15.883	15.876
2MASS1523+30	L8	16.102	15.984	16.039	16.093	16.041	15.950	16.066	16.069
SDSS0032+14	L8	16.733	16.609	16.670	16.724	16.672	16.581	16.695	16.686
SDSS0857+57	L8	14.956	14.830	14.891	14.945	14.893	14.800	14.916	14.910
2MASS0310+16	L9	15.996	15.873	15.934	15.986	15.936	15.838	15.957	15.960
SDSS0830+48	L9	15.389	15.265	15.324	15.379	15.326	15.223	15.354	15.369
2MASS0328+23	L9.5	16.511	16.383	16.445	16.499	16.448	16.350	16.472	16.475
SDSS0423−04	T0	14.466	14.342	14.400	14.455	14.401	14.301	14.430	14.451
SDSS0837−00	T0.5	17.079	16.949	17.006	17.061	17.006	16.902	17.038	17.084
SDSS0151+12	T1	16.424	16.298	16.354	16.409	16.355	16.251	16.387	16.427
SDSS1254−01	T2	14.873	14.724	14.791	14.852	14.793	14.661	14.833	14.893
SDSS1021−03	T3	16.115	15.948	16.026	16.088	16.030	15.880	16.069	16.128
SDSS1750+17	T3.5	16.358	16.210	16.281	16.340	16.284	16.139	16.322	16.388
2MASS0559−14	T4.5	13.829	13.648	13.731	13.797	13.735	13.571	13.777	13.851
SDSS0207+00	T4.5	16.886	16.709	16.791	16.855	16.796	16.631	16.838	16.915
SDSS0926+58	T4.5	15.714	15.546	15.622	15.680	15.627	15.468	15.669	15.750
2MASS1225−27AB	T6	15.173	14.963	15.061	15.130	15.070	14.879	15.116	15.197
GL229B	T6	14.324	14.087	14.195	14.275	14.204	14.007	14.255	14.323
SDSS1110+01	T6	16.411	16.202	16.301	16.367	16.310	16.121	16.354	16.433
SDSS1346−00	T6	15.810	15.582	15.685	15.758	15.694	15.493	15.745	15.821
SDSS1624+00	T6	15.513	15.287	15.390	15.466	15.398	15.197	15.449	15.539
2MASS1217−03	T8	15.900	15.652	15.769	15.841	15.780	15.562	15.827	15.916
GL570D	T8	15.101	14.846	14.966	15.039	14.978	14.755	15.029	15.114
2MASS0415−09	T9	15.687	15.414	15.542	15.625	15.556	15.321	15.611	15.695

Table 2. Synthesized H-Band Photometry

Name	Type	2MASS	CIT	LCO	MKO	NOFS	UKIRT
2MASS0345+25	L1	13.169	13.195	13.197	13.208	13.157	13.144
2MASS0746+20AB	L1	10.943	10.970	10.972	10.984	10.931	10.917
2MASS0028+15	L3	15.514	15.550	15.553	15.570	15.498	15.479
DENIS1058−15	L3	13.232	13.266	13.269	13.286	13.214	13.196
GD165B	L3	14.705	14.737	14.739	14.749	14.696	14.686
Kelu−1	L3	12.402	12.435	12.437	12.452	12.388	12.371
2MASS0036+18	L4	11.547	11.583	11.585	11.598	11.536	11.522
SDSS0539−00	L5	12.991	13.028	13.030	13.040	12.983	12.970
SDSS1257−01	L5	14.642	14.679	14.681	14.693	14.631	14.620
SDSS1446+00	L5	14.536	14.572	14.575	14.588	14.523	14.508
SDSS2249+00	L5	15.366	15.403	15.407	15.428	15.345	15.319
DENIS0205−11AB	L5.5	13.552	13.592	13.593	13.604	13.545	13.535
SDSS0107+00	L5.5	14.506	14.540	14.543	14.561	14.486	14.464
SDSS1326−00	L5.5	14.968	15.004	15.007	15.024	14.950	14.930
2MASS0825+21	L6	13.755	13.790	13.792	13.810	13.738	13.718
DENIS1228−15AB	L6	13.354	13.394	13.395	13.408	13.344	13.330
SDSS0236+00	L6.5	15.112	15.149	15.151	15.161	15.105	15.093
2MASS1632+19	L7.5	14.683	14.720	14.723	14.737	14.669	14.652
2MASS1523+30	L8	15.008	15.048	15.050	15.064	14.997	14.982
SDSS0032+14	L8	15.609	15.648	15.650	15.663	15.599	15.585
SDSS0857+57	L8	13.755	13.794	13.796	13.813	13.740	13.721
2MASS0310+16	L9	14.852	14.893	14.895	14.911	14.839	14.820
SDSS0830+48	L9	14.345	14.391	14.393	14.402	14.341	14.329
2MASS0328+23	L9.5	15.432	15.471	15.472	15.483	15.426	15.416
SDSS0423−04	T0	13.456	13.498	13.499	13.510	13.449	13.438
SDSS0837−00	T0.5	16.155	16.201	16.202	16.210	16.153	16.145
SDSS0151+12	T1	15.484	15.531	15.532	15.540	15.482	15.473
SDSS1254−01	T2	14.070	14.121	14.120	14.130	14.069	14.064
SDSS1021−03	T3	15.376	15.428	15.425	15.432	15.377	15.381
SDSS1750+17	T3.5	15.894	15.943	15.939	15.939	15.905	15.921
2MASS0559−14	T4.5	13.595	13.646	13.639	13.641	13.603	13.628
SDSS0207+00	T4.5	16.581	16.634	16.628	16.634	16.586	16.603
SDSS0926+58	T4.5	15.400	15.454	15.446	15.449	15.408	15.434
2MASS1225−27AB	T6	15.131	15.183	15.171	15.169	15.143	15.192
GL229B	T6	14.337	14.380	14.365	14.358	14.353	14.412
SDSS1110+01	T6	16.187	16.234	16.223	16.222	16.196	16.243
SDSS1346−00	T6	15.797	15.851	15.838	15.839	15.804	15.850
SDSS1624+00	T6	15.441	15.496	15.485	15.482	15.453	15.496
2MASS1217−03	T8	15.942	15.999	15.980	15.978	15.954	16.026
GL570D	T8	15.240	15.300	15.281	15.280	15.252	15.323
2MASS0415−09	T9	15.652	15.718	15.697	15.697	15.665	15.740

Table 3. Synthesized K-Band Photometry

Name	Type	2MASS	CIT	DENIS	LCO	MKO	NOFS	UKIRT
2MASS0345+25	L1	12.693	12.672	12.706	12.674	12.663	12.685	12.699
2MASS0746+20AB	L1	10.464	10.475	10.479	10.481	10.452	10.486	10.499
2MASS0028+15	L3	14.609	14.579	14.627	14.580	14.573	14.595	14.616
DENIS1058−15	L3	12.603	12.573	12.615	12.574	12.568	12.588	12.603
GD165B	L3	14.116	14.101	14.134	14.105	14.088	14.116	14.135
Kelu−1	L3	11.820	11.788	11.835	11.789	11.780	11.803	11.820
2MASS0036+18	L4	11.067	11.063	11.083	11.069	11.045	11.077	11.094
SDSS0539−00	L5	12.427	12.409	12.446	12.413	12.400	12.423	12.445
SDSS1257−01	L5	14.081	14.061	14.100	14.065	14.051	14.076	14.097
SDSS1446+00	L5	13.832	13.811	13.851	13.814	13.803	13.827	13.848
SDSS2249+00	L5	14.478	14.432	14.493	14.431	14.433	14.448	14.467
DENIS0205−11AB	L5.5	12.977	12.982	13.000	12.990	12.965	12.996	13.019
SDSS0107+00	L5.5	13.630	13.587	13.645	13.587	13.592	13.602	13.623
SDSS1326−00	L5.5	14.116	14.074	14.132	14.074	14.076	14.089	14.110
2MASS0825+21	L6	12.961	12.924	12.980	12.925	12.928	12.939	12.963
DENIS1228−15AB	L6	12.741	12.725	12.760	12.729	12.713	12.740	12.760
SDSS0236+00	L6.5	14.559	14.546	14.579	14.551	14.540	14.559	14.581
2MASS1632+19	L7.5	13.935	13.921	13.955	13.923	13.913	13.933	13.956
2MASS1523+30	L8	14.358	14.348	14.378	14.352	14.343	14.360	14.384
SDSS0032+14	L8	14.999	15.003	15.022	15.010	14.990	15.014	15.039
SDSS0857+57	L8	12.960	12.932	12.980	12.934	12.932	12.947	12.971
2MASS0310+16	L9	14.192	14.240	14.217	14.252	14.202	14.250	14.273
SDSS0830+48	L9	13.702	13.691	13.728	13.699	13.679	13.707	13.735
2MASS0328+23	L9.5	14.869	14.870	14.891	14.874	14.860	14.881	14.906
SDSS0423−04	T0	12.974	12.968	12.996	12.973	12.960	12.980	13.005
SDSS0837−00	T0.5	15.960	15.997	15.991	16.005	15.978	16.006	16.037
SDSS0151+12	T1	15.164	15.195	15.191	15.204	15.180	15.204	15.232
SDSS1254−01	T2	13.800	13.870	13.833	13.883	13.839	13.875	13.910
SDSS1021−03	T3	15.193	15.265	15.225	15.278	15.238	15.269	15.302
SDSS1750+17	T3.5	15.942	16.073	15.980	16.095	16.021	16.069	16.108
2MASS0559−14	T4.5	13.634	13.800	13.676	13.829	13.743	13.788	13.829
SDSS0207+00	T4.5	16.504	16.721	16.549	16.757	16.636	16.704	16.747
SDSS0926+58	T4.5	15.367	15.515	15.408	15.547	15.464	15.505	15.550
2MASS1225−27AB	T6	15.153	15.350	15.203	15.394	15.282	15.334	15.384
GL229B	T6	14.275	14.435	14.318	14.476	14.366	14.424	14.463
SDSS1110+01	T6	15.941	16.097	15.970	16.120	16.039	16.067	16.085
SDSS1346−00	T6	15.607	15.810	15.653	15.854	15.736	15.784	15.835
SDSS1624+00	T6	15.484	15.669	15.530	15.704	15.608	15.653	15.698
2MASS1217−03	T8	15.760	16.016	15.812	16.073	15.924	15.989	16.035
GL570D	T8	15.379	15.607	15.430	15.661	15.524	15.585	15.631
2MASS0415−09	T9	15.679	15.909	15.733	15.970	15.823	15.888	15.942

Table 4. Coefficients of Cubic Fit[a] to [δmag, Spectral Type]

System	Filter	Coefficient$_0$	Coefficient$_1$	Coefficient$_2$	Coefficient$_3$	Error[b]
2MASS	J	+0.121	−1.64e−3	+6.32e−4	+9.01e−6	4.5e−3
2MASS	H	−0.034	−6.88e−3	+6.27e−4	−1.43e−5	1.1e−3
2MASS	K	−0.004	+2.04e−2	−2.80e−3	+6.75e−5	7.8e−3
CIT	J	+0.020	−3.97e−3	+9.20e−4	−2.64e−5	0.6e−3
CIT	H	−0.009	−3.69e−3	+4.22e−4	−6.92e−6	0.5e−3
CIT	K	+0.023	−7.39e−3	+8.11e−4	−1.17e−5	2.3e−3
ELIAS	J	+0.066	−1.16e−3	+5.45e−4	−1.57e−6	1.4e−3
DENIS	J	+0.112	−1.16e−3	+6.33e−4	−1.21e−6	3.2e−3
DENIS	K	+0.011	+1.99e−2	−2.60e−3	+6.44e−5	5.8e−3
LCO	J	+0.065	−4.82e−4	+4.52e−4	+3.74e−6	1.7e−3
LCO	H	−0.008	−3.11e−3	+4.00e−4	−1.09e−5	0.3e−3
LCO	K	+0.034	−1.13e−2	+1.22e−3	−1.47e−5	6.3e−3
NOFS	J	+0.085	−3.27e−3	+9.62e−4	−1.07e−5	2.5e−3
NOFS	H	−0.041	−1.08e−2	+1.21e−3	−3.11e−5	2.5e−3
NOFS	K	+0.034	−5.27e−3	+5.65e−4	−1.07e−5	2.8e−3
UKIRT	J	+0.089	−1.67e−2	+3.23e−3	−8.11e−5	5.3e−3
UKIRT	H	−0.048	−1.44e−2	+1.45e−3	−1.96e−5	6.7e−3
UKIRT	K	+0.048	−4.15e−3	+5.96e−4	−9.94e−6	5.0e−3

[a]Fit is applied as

$$mag_{system} - mag_{MKO} = Coeff_0 + Coeff_1 \times Type + Coeff_2 \times Type^2 + Coeff_3 \times Type^3$$

where type is an integer such that 01=L1, 10=T0, 19=T9

[b]RMS scatter of the fit in magnitudes

Table 5. Coefficients of Quadratic Fit[a] to [$\delta Jmag$, $J-K$]

System	Filter	Coefficient$_0$	Coefficient$_1$	Coefficient$_2$	Error[b]	$J-K_{system}$
2MASS	J	+0.261	−1.29e−01	+3.35e−02	+2.01e−02	MKO
CIT	J	+0.073	−3.55e−02	+4.09e−03	+3.58e−03	MKO
ELIAS	J	+0.160	−8.01e−02	+1.95e−02	+8.85e−03	MKO
DENIS	J	+0.223	−9.48e−02	+2.35e−02	+1.37e−02	MKO
LCO	J	+0.165	−8.79e−02	+2.23e−02	+1.02e−02	MKO
NOFS	J	+0.208	−1.04e−01	+2.40e−02	+1.60e−02	MKO
UKIRT	J	+0.278	−1.41e−01	+1.93e−02	+3.77e−02	MKO
			$J-K_{other}$			
2MASS	J	+0.325	−1.93e−01	+4.97e−02	+2.54e−02	2MASS
CIT	J	+0.074	−3.56e−02	+4.20e−03	+3.74e−03	CIT
ELIAS	J	+0.168	−8.74e−02	+2.11e−02	+9.43e−03	ELIAS
DENIS	J	+0.257	−1.29e−01	+3.26e−02	+1.57e−02	DENIS
LCO	J	+0.172	−9.26e−02	+2.31e−02	+1.08e−02	LCO
NOFS	J	+0.227	−1.22e−01	+2.84e−02	+1.79e−02	NOFS
UKIRT	J	+0.308	−1.68e−01	+2.61e−02	+4.58e−02	UKIRT

[a]Fit is applied as

$$mag_{system} - mag_{MKO} = Coeff_0 + Coeff_1 \times J-K_{system} + Coeff_2 \times J-K^2_{system}$$

where $J-K_{system}$ is the observed color in the photometric system of the 7th column

[b]RMS scatter of the fit in magnitudes

Table 6. Coefficients of Linear Fit[a] to [δH,$\delta Kmag$, $J-K$]

System	Filter	intercept	err_{int}	gradient	err_{grad}	$J-K_{system}$
2MASS	H	−0.043	+0.001	−6.49e−03	+1.07e−03	MKO
2MASS	K	−0.096	+0.004	+7.31e−02	+3.23e−03	MKO
CIT	H	+0.009	+0.001	−1.52e−02	+6.27e−04	MKO
CIT	K	+0.060	+0.002	−3.13e−02	+1.70e−03	MKO
DENIS	K	−0.056	+0.004	+5.99e−02	+2.66e−03	MKO
LCO	H	−0.002	+0.001	−7.46e−03	+4.17e−04	MKO
LCO	K	+0.093	+0.004	−5.00e−02	+2.66e−03	MKO
NOFS	H	−0.036	+0.002	−1.83e−02	+1.21e−03	MKO
NOFS	K	+0.048	+0.002	−1.56e−02	+1.40e−03	MKO
UKIRT	H	+0.000	+0.003	−5.00e−02	+2.50e−03	MKO
UKIRT	K	+0.083	+0.004	−2.40e−02	+3.04e−03	MKO
			$J-K_{other}$			
2MASS	H	−0.040	+0.002	−7.77e−03	+1.25e−03	2MASS
2MASS	K	−0.126	+0.007	+8.34e−02	+4.62e−03	2MASS
CIT	H	+0.009	+0.001	−1.52e−02	+6.25e−04	CIT
CIT	K	+0.060	+0.002	−3.13e−02	+1.66e−03	CIT
DENIS	K	−0.074	+0.005	+6.74e−02	+3.44e−03	DENIS
LCO	H	−0.001	+0.001	−7.49e−03	+4.24e−04	LCO
LCO	K	+0.097	+0.004	−5.03e−02	+2.65e−03	LCO
NOFS	H	−0.032	+0.002	−1.94e−02	+1.27e−03	NOFS
NOFS	K	+0.051	+0.002	−1.66e−02	+1.46e−03	NOFS
UKIRT	H	+0.009	+0.004	−5.41e−02	+2.82e−03	UKIRT
UKIRT	K	+0.087	+0.005	−2.54e−02	+3.42e−03	UKIRT

[a]Fit is applied as

$$mag_{system} - mag_{MKO} = intercept \pm err_{int} + gradient \pm err_{grad} \times J - K_{system}$$

where $J-K_{system}$ is the observed color in the photometric system of the 7th column